

# Spontaneous symmetry breaking and discontinuous phase transition for spreading dynamics in multiplex networks

Ningbo An<sup>1</sup>, Hanshuang Chen<sup>2,\*</sup>, Chuang Ma<sup>1</sup>, and Haifeng Zhang<sup>1</sup>

<sup>1</sup>*School of Mathematical Science, Anhui University, Hefei, 230601, China*

<sup>2</sup>*School of Physics and Materials Science, Anhui University, Hefei, 230601, China*

(Dated: August 1, 2019)

We propose a spreading model in multilayer networks and study the nature of nonequilibrium phase transition in the model. The model integrates the susceptible-infected-susceptible (or susceptible-infected-recovered) spreading dynamics with a biased diffusion process among different layers. A parameter  $\alpha$  is introduced to control the bias of the diffusion process, such that each individual prefers to move to one layer with more infected (or recovered) neighbors for larger values of  $\alpha$ . Using stochastic simulations and mean-field theory, we show that the type of phase transition from a disease-free phase to an endemic phase depends on the value of  $\alpha$ . When  $\alpha$  is small enough, the system undergoes a usual continuous phase transition as an effective spreading rate  $\beta$  increases, as in single-layer networks. Interestingly, when  $\alpha$  exceeds a critical value the system shows either a hybrid two-step phase transition or a one-step discontinuous phase transition as  $\beta$  increases. The former contains a continuous transition between the disease-free phase and a low-prevalence endemic phase, and a discontinuous transition between the low-prevalence endemic phase and a high-prevalence endemic phase. For the latter, only a discontinuous transition occurs from the disease-free phase directly to the high-prevalence endemic phase. Moreover, we show that the discontinuous transition is always accompanied by a spontaneous symmetry breaking in occupation probabilities of individuals in each layer.

## I. INTRODUCTION

Over the past two decades, we have witnessed the power of network science on modeling dynamical processes in complex systems made of large numbers of interacting elements [1–5]. In particular, considerable attention has been devoted to the phase transitions and critical phenomena in complex networks [6]. Owing to the inherent randomness and heterogeneity in the interacting patterns, some nontrivial phenomena have been revealed, such as the anomalous behavior of Ising model [7–9] to a vanishing percolation threshold [10, 11] and the absence of epidemic thresholds that separate healthy and endemic phases [12] as well as explosive emergence of phase transitions [13–15].

However, the vast majority of the previous works considered dynamical processes in single-layer networks. In fact, many real-world complex systems are usually composed of intertwined multilayer networks [16, 17]. It has now been recognized that the study of multilayer networks is fundamental for enhancing understanding of dynamical processes in networked systems [18]. A seminal work from Buldyrev et al. [19] showed the catastrophic effect of failure in an interdependent networks of power grids and computers. Baxter et al. [20] showed that percolation transition in multiplex networks can be discontinuous and a first-order-like, in contrast to that in single-layer networks. Gómez et al. [21] studied a linear diffusion in multilayer networks and showed that the multiplex structure is able to speed up the less diffusive of separated layers. The diffusive properties are

related to a structural transition of the multiplex from a decoupled regime to a systemic regime [22]. In particular, some works focused on spreading processes in multilayer networks [23–25]. Cozzo et al. [26] showed that the epidemic threshold of the susceptible-infected-susceptible (SIS) model in a multilayer network is always smaller than that in any isolated network. Wang et al. [27] further showed that the epidemic threshold can be reduced dramatically when two nodes with dominant eigenvector components of the adjacency matrices of isolated networks are linked. Similar results were also obtained by a degree-based mean-field approach [28]. However, based on the percolation theory [29], Dickison et al. [30] unveiled one important difference in the susceptible-infected-recovered (SIR) model with respect to the SIS dynamics when the coupling between layers is weak. Spreading processes in structured metapopulations can be well characterized within the framework of multilayer networks as well [31–33]. In addition, a variety of dynamics has also been investigated, such as evolutionary games [34–36], synchronization [37–39], opinion formation [40, 41], and transportation [42, 43].

The multiplex structure also provides a convenient framework for studying the interplay between different dynamical processes. Granell et al. [44] coupled the SIS spreading taking place on a physical network with another stochastic Aware-Unaware dynamics in a virtual network. They showed that the infected agents trigger the mechanism of awareness in the virtual layer, and thus decreases the incidence of the disease and increases the epidemic onset. Kan et al. [45] considered that susceptible individuals can be informed not only from other aware individuals through the information network, but also become self-awareness induced by the infected neighbors in

---

\* chenhsf@ahu.edu.cn

contact network. They showed that the introduction of the self-awareness can lower the density of infection, but cannot increase the epidemic threshold. Wang et al. [46] proposed an asymmetrically interacting bilayer network model to elucidate the interplay between information diffusion and epidemic spreading, and they showed that the outbreak of the information can be triggered not only by its own spreading dynamics but also by the epidemic outbreak on the counter-layer. Zhang et al. [47] observed a spontaneous explosive synchronization via adaptively controlling the links in terms of a local order parameter in single-layer and multilayer networks. Nicosia et al. [48] showed that the interactions between synchronization and transport dynamics can also induce a spontaneous explosive synchronization in multiplex networks.

Very recently, discontinuous phase transition of the spreading model in multiplex networks has received growing attention. Velásquez-Rojas and Vazquez [49] coupled contact process for disease spreading with the voter model for opinion formation take place on two layers of networks, and they showed that a continuous transition in the contact process becomes discontinuous as the infection probability increases beyond a threshold. Pires et al. [50] proposed an SIS-like model with an extra vaccinated state, in which individuals vaccinate with a probability proportional to their opinions. Meanwhile, individuals update their opinions in terms of peer influence. They also observed a first-order active-absorbing phase transition in the model. Jiang and Zhou [51] studied the effect of resource amount on epidemic control in a modified SIS model on a two-layer network, and they found that the spreading process goes through a first-order phase transition if the infection strength between layers is weak. Su et al. [52] proposed a reversible social contagion model of community networks that includes the factor of social reinforcement. They showed that the model exhibits a first-order phase transition in the spreading dynamics, and that a hysteresis loop emerges in the system when there is a variety of initially adopted seeds. Chen et al. [53] studied the dynamics of the SIS model in social-contact multiplex networks when the recovery of infected nodes depends on resources from healthy neighbors in the social layer. They found that as the infection rate increases the infected density varies smoothly from zero to a finite small value and then suddenly jumps to a high value, where a hysteresis phenomenon was also observed.

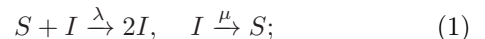
In this work, we propose a spreading model in multiplex networks and study, both in simulations and theoretically, the nature of phase transition from a healthy phase to an endemic phase. In the model, each individual updates its state via the SIS (or SIR) dynamics and simultaneously performs a biased diffusion from one layer to the other depending on the number of infected (or recovered) neighbors in the target layer. We show that the type of phase transition depends on the value  $\alpha$  of a parameter that controls the degree of the biased diffusion. For small values of  $\alpha$ , the phase transition is customarily continuous or second-order. For intermediate values of

$\alpha$ , the phase transition is hybrid. The system first undergoes a continuous transition from the healthy phase to a low-prevalence endemic phase and then to a high-prevalence endemic phase in an abrupt way. For large values of  $\alpha$ , the model solely shows a discontinuous or first-order-like transition from the healthy phase to the high-prevalence endemic phase. We attribute the mechanism of the novel discontinuous phase transition to a spontaneous symmetry breaking in occupation probabilities of individuals in each layer.

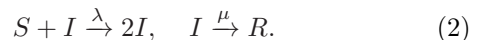
The organization of this paper is as follows. We present the definition of the model and simulation details in section II. Main results for the SIS and SIR dynamics are presented in section III and section IV, respectively. We conclude with the summary of the results in section V.

## II. MODEL AND SIMULATION DETAILS

Let us define our model in multiplex networks as follows. The network is consisted of  $\mathcal{L}$  layers. Each layer contains the same number of nodes,  $N$ , and there exists a one-to-one correspondence between nodes in different layers. The topology in each layer is described by an adjacency matrix  $\mathbf{A}^\ell$  ( $\ell = 1, \dots, \mathcal{L}$ ), whose entries  $A_{ij}^\ell$  are defined as  $A_{ij}^\ell = 1$  if there is an edge from node  $j$  to node  $i$  in the  $\ell$ -th layer, and  $A_{ij}^\ell = 0$  otherwise. Note that the topology at each layer may be different. In time  $t$ , each individual  $i$  can be located at one of layers, denoted by a variable  $v_i(t) \in \{1, \dots, \mathcal{L}\}$ . The dynamics in multiplex networks is consisted of an epidemic spreading process and a diffusion process of individuals among layers. We will use the two most paradigmatic epidemic models, the SIS model and SIR model. The two models can be described by the following reactions,



for the reversible SIS model, while for the irreversible SIR model,



Here  $\lambda$  is the spreading rate that a susceptible individual is infected when contacting with a single infected individual, and  $\mu$  is the recovering rate that an infected is recovered and turns to be susceptible again (SIS) or becomes immunized (SIR). For convenience, we denote the state of each individual  $i$  at time  $t$  by a variable  $\sigma_i(t) \in \{S, I\}$  for the SIS model and  $\sigma_i(t) \in \{S, I, R\}$  for the SIR model. To proceed Monte Carlo simulation, we discretize the time with a step  $\Delta t$  for the dynamical evolutions. In the subsequent time  $t + \Delta t$ , all nodes synchronously update their states and locations according to the following two steps.

(i) Spreading process. If the individual  $i$  is susceptible at time  $t$ ,  $\sigma_i(t) = S$ , it becomes infective by contacting with infected individuals of the same layer. Since the probability that the individual  $i$  is infected by each

infective individual of the same layer is  $\lambda\Delta t$ , the probability that the individual  $i$  is infected at the time  $t + \Delta t$  providing that (s)he is susceptible at time  $t$  is written as

$$P(\sigma_i(t + \Delta t) = I | \sigma_i(t) = S) = \lambda n_i(t) \Delta t, \quad (3)$$

where  $n_i(t)$  is the number of infective individuals at the same layer as the individual  $i$  at the time  $t$ . Providing that the individual  $i$  is infective at time  $t$ ,  $\sigma_i(t) = I$ , on the other hand, (s)he becomes spontaneously susceptible for the SIS model (or immunized for the SIR model) at the time  $t + \Delta t$  with a probability  $\mu\Delta t$ , i.e.,

$$P(\sigma_i(t + \Delta t) = S/R | \sigma_i(t) = I) = \mu\Delta t. \quad (4)$$

(ii) *Diffusion* process. Each individual  $i$  tries to perform a random diffusion to some layer with the probability  $D\Delta t$  with the diffusion rate  $D$ . Otherwise, the individual  $i$  still stays in its original layer. If a diffusion process happens, a target layer needs to be chosen in advance. To this end, we suppose that the probability that the individual  $i$  moves to some layer depends on the number of infected individuals for the SIS model (or the number of recovered individuals for the SIR model) among its neighborhoods in such a layer. To formulate this process, we define the probability that the  $\ell$ -th layer is selected as the target layer of the individual  $i$  (including the original layer of the individual  $i$ ) as

$$T_i^\ell(t) = \begin{cases} \frac{\exp[\alpha n_{i,\ell}(t)]}{\sum_{\ell'} \exp[\alpha n_{i,\ell'}(t)]}, & \text{for SIS model} \\ \frac{\exp[\alpha n_{r,\ell}(t)]}{\sum_{\ell'} \exp[\alpha n_{r,\ell'}(t)]}, & \text{for SIR model} \end{cases} \quad (5)$$

where the denominator is a normalization factor and  $\alpha$  is a tunable parameter that controls the preference on the choice of the target layer.  $n_{i,\ell}(t)$  ( $n_{r,\ell}(t)$ ) is the number of infected (recovered) individuals among the neighborhoods of the individual  $i$  in the  $\ell$ -th layer at the time  $t$ . If  $\alpha = 0$ , each layer has an equal probability to be chosen as the target layer [54]. If  $\alpha > 0$ , the individual prefers to choose the layer with more infected (or recovered) individuals among its neighborhoods as the target layer for the SIS (or SIR) model. Instead, if  $\alpha < 0$  individuals prefer to choose the layer with less infected or recovered individuals. The larger the absolute value of  $\alpha$  is, the stronger degree of the preference has. The case  $\alpha > 0$  may be related to the spreading dynamics of some virtual information, such as interest for some product or scientific research topic. While for the spreading of a real epidemic, one always tries to avoid infection by moving to layers with the smaller number of infected individuals, which corresponds to the case  $\alpha < 0$ . Finally, the probability of the individual  $i$  moving to the  $\ell$ -th layer at the time  $t + \Delta t$  can be written as

$$P(v_i(t + \Delta t) = \ell) = \begin{cases} 1 - D\Delta t + T_i^\ell(t) D\Delta t, & \ell = v_i(t); \\ T_i^\ell(t) D\Delta t, & \ell \neq v_i(t). \end{cases} \quad (6)$$

We also used other forms of Eq.(5) such as a power-law function,  $T_i^\ell \propto n_{i(r),\ell}^\alpha$ , and found the main conclusions

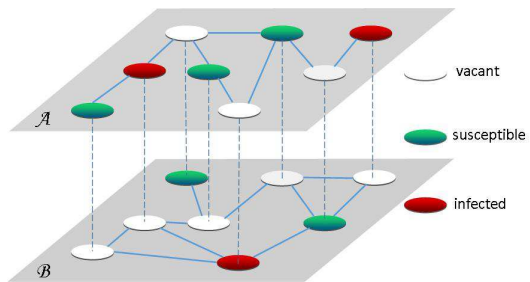


FIG. 1. A schematic of our model with the SIS dynamics in a two-layer network. Each individual stays either in layer  $\mathcal{A}$  or in layer  $\mathcal{B}$ . If an individual stays in layer  $\mathcal{A}$  at a certain moment, (s)he is vacant in layer  $\mathcal{B}$  at the moment. The state of each individual is either susceptible (S) or infected (I). The evolution of the states and locations of all the individuals are governed by the SIS spreading dynamics (Eq.(3) and Eq.(4)) and diffusion processes (Eq.(6)), respectively.

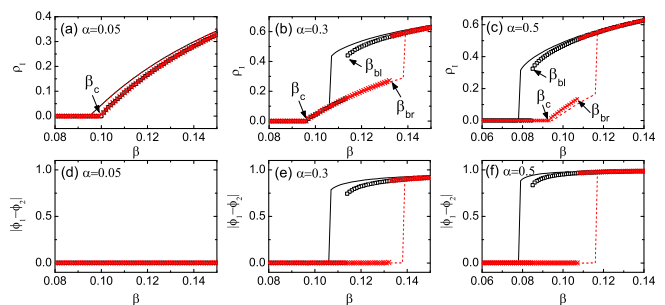


FIG. 2. The density of infected individuals  $\rho_I$  (top panels) and  $|\phi_1 - \phi_2|$  (bottom panels) as functions of the effective spreading rate  $\beta$  in a two-layer network for three distinct values of  $\alpha$ : 0.05, 0.3, and 0.5 (from left to right). Each layer is consisted of an identical ER network with  $N = 5 \times 10^4$  nodes and average degree ( $k$ ) = 20. All the results are obtained from two different initial conditions:  $\rho(0) = 0.1$  and  $|\phi_1(0) - \phi_2(0)| = 1$  (squares and solid lines);  $\rho(0) = 0.1$  and  $|\phi_1(0) - \phi_2(0)| = 0$  (crosses and dotted lines). The symbols and lines correspond to simulation and theoretical results, respectively.

shown below hold as well. A schematic of our model with the SIS dynamics in a two-layer network is shown in Fig.1.

In the simulations, we set  $\mu = 1$ ,  $D = 10$  and  $\Delta t = 0.05$  unless otherwise specified. We have also tested other sets of parameters and found that the results are essentially the same. We define a dimensionless quantity  $\beta = \lambda/\mu$  as the effective spreading parameter, and  $\rho_{\{I,R\}}(t)$  as the fraction of the infected (recovered) individuals at time  $t$ . Furthermore, we define  $\phi_\ell(t)$  as the occupation probability of individuals in the  $\ell$ -th layer at time  $t$ . Before the simulation, we randomly choose a fraction  $\rho_I(0)$  of individuals as the seeds of the spreading, i.e., these seeded individuals are initially set to be infective and the remaining individuals to be susceptible. The initial locations of all the individuals are prepared with three distinct cases: (i)  $\phi_1(0) = \phi_2(0) = 0.5$ ; (ii)  $\phi_1(0) = 0$ ,  $\phi_2(0) = 1$ , and

(iii)  $\phi_1(0) = 1, \phi_2(0) = 0$ . To achieve the stationary values of  $\rho_{\{I,R\}}$  and  $\phi_\ell$ , we generate 20 random realizations for a given initial condition. In each realization, the simulation is run up to  $t = 10^3$  and the last  $t = 5 \times 10^2$  is used to compute the averages.

### III. SIS DYNAMICS

We start from a two-layer network. Each layer is consisted of an identical Erdős-Rényi (ER) network with  $N = 5 \times 10^4$  nodes and average degree  $\langle k \rangle = 20$  [55]. The initial density of infected seeds is set to be  $\rho_I(0) = 0.1$ . Figure 2 shows  $\rho_I$  (top panels) and  $|\phi_1 - \phi_2|$  (bottom panels) as functions of  $\beta$  for three distinct values of  $\alpha$ : 0.05, 0.3, and 0.5 (from left to right). Since the topologies in all layers are exactly the same, the initial conditions (ii) and (iii) produce the same results. Later, we will discuss the general case when the networks in each layer are not the same. For  $\alpha = 0.05$  (Fig.2(a)), one sees that the results for two different initial conditions coincide with each other, implying that the system undergoes a usual continuous second-order phase transition from a healthy phase (HP) to an endemic phase (EP) as  $\beta$  increases, separated by a threshold value of  $\beta_c$ . This is qualitatively the same as the SIS dynamics in single-layer networks. Quantitatively, the threshold is raised for the multi-layer case. This is because that all the individuals stays in each layer with equal probabilities (Fig.2(d)) and therefore the bilayer network can be considered to be two separated percolated networks with site occupied probability 0.5. In such percolated networks, the degree of each node is reduced on average by half. It is known that a simple mean-field calculation predicts that epidemic threshold equals to the inverse of the average degree of network [4]. Thus, the value of epidemic threshold in the bilayer network is expected to be twice that of a single layer with the same average degree [54]. Below we shall show the conclusion also holds by using an individual-based mean-field method (see Eq.(15) and Eq.(16)).

Interestingly, for  $\alpha = 0.3$  (Fig.2(b)), the system first undergoes a continuous transition from HP to a low-prevalence endemic phase (L-EP) at  $\beta = \beta_c$ , and then shows a discontinuous transition to a high-prevalence endemic phase (H-EP) at  $\beta = \beta_b$ . The location of  $\beta_b$  depends on the distribution of initial positions of individuals. When the initial condition (i) is used, the discontinuous transition point occurs at  $\beta = \beta_{br}$ , and at  $\beta = \beta_{bl}$  while the initial condition (ii) or (iii) is used. These two discontinuous transition points,  $\beta_{bl}$  and  $\beta_{br}$  ( $\beta_{bl} < \beta_{br}$ ), do not coincide and thus forms a bistable region, a typical characteristic of a first-order phase transition. Within this bistable region, the prevalence is either low or high depending on the initial condition. Specially, if all the individuals are evenly placed in each layer initially, the final stationary density of infected individuals is low. If most of the individuals are placed on some one layer initially, the density is high. Moreover, we should note that

such a discontinuous transition in  $\rho_I$  is accompanied by a symmetry breaking in occupation probabilities of individuals in each layer (Fig.2(e)). Prior to the discontinuous transition happening, the occupation probabilities are symmetry,  $\phi_1 = \phi_2$ . Across the discontinuous transition, the symmetry is broken and the occupation probabilities become seriously uneven,  $\phi_1 \neq \phi_2$ .

For  $\alpha = 0.5$  (Fig.2(c)), we find that, as compared to  $\alpha = 0.3$ , the case is similar if the initial condition (i) is used, but is significantly different if the initial condition (ii) or (iii) is adopted. For the latter, the system shows the solely discontinuous transition from the HP to the H-EP at  $\beta = \beta_{bl}$ . Thus, we can divide the bistable region into two subregions. In the left subregion ( $\beta_{bl} < \beta < \beta_c$ ), the HP and the H-EP coexist (named as bistable phase 1 (BP1)). In the right one ( $\beta_c < \beta < \beta_{br}$ ), the L-EP and the H-EP coexist (called BP2). Also, the symmetry broken in the occupation probabilities happens at both boundaries of the bistable region (Fig.2(f)).

We have also investigated the case when  $\alpha < 0$ . We found that the outbreak of the epidemic is always continuous and the occupation probabilities in each layer are the same. While the epidemic threshold increases slowly as  $\alpha$  decreases, such a case does not bring any qualitative change in the nature of phase transition. Therefore, in the following we will focus on the case only when  $\alpha \geq 0$ .

The bistability always implies the coexistence of two or more distinct stable phases within the bistable region. Intuitively speaking, its origin in our model stems from the the interaction between spreading dynamics and diffusion in a nonlinear way. To seek a theoretical interpretation, we define  $\rho_{I,i}(t)$  as the probability that the individual  $i$  is infected at time  $t$ , and  $w_{i,\ell}(t)$  as the probability that the individual  $i$  locates at the  $\ell$ -th layer at time  $t$ . The time evolution for  $\rho_{I,i}(t)$  reads,

$$\rho_{I,i}(t + \Delta t) = [1 - \rho_{I,i}(t)] q_i(t) \Delta t + (1 - \mu \Delta t) \rho_{I,i}(t), \quad (7)$$

where  $q_i(t)$  is the infection rate of the individual  $i$  at time  $t$ , given by

$$q_i(t) = \lambda \sum_{j=1}^N \rho_{I,j}(t) \sum_{\ell=1}^{\mathcal{L}} A_{ij}^{\ell} w_{i,\ell}(t) w_{j,\ell}(t). \quad (8)$$

The time evolution for  $w_{i,\ell}$  is written as

$$w_{i,\ell}(t + \Delta t) = (1 - D \Delta t) w_{i,\ell}(t) + \sum_{\ell'=1}^{\mathcal{L}} w_{i,\ell'}(t) T_i^{\ell}(t) D \Delta t. \quad (9)$$

Utilizing the normalization condition  $\sum_{\ell=1}^{\mathcal{L}} w_{i,\ell}(t) = 1$ , Eq.(9) can be rewritten as

$$w_{i,\ell}(t + \Delta t) = (1 - D \Delta t) w_{i,\ell}(t) + T_i^{\ell} D \Delta t. \quad (10)$$

In the continuous time limit,  $\Delta t \rightarrow 0$ , Eq.(7) and Eq.(10) can be rewritten as ordinary differential equations,

$$\frac{d\rho_{I,i}(t)}{dt} = (1 - \rho_{I,i}(t)) q_i(t) - \mu \rho_{I,i}(t), \quad (11)$$

and

$$\frac{dw_{i,\ell}(t)}{dt} = -Dw_{i,\ell}(t) + DT_i^\ell(t). \quad (12)$$

In the steady state,  $d\rho_{I,i}(t)/dt = 0$  and  $dw_{i,\ell}(t)/dt = 0$ , we have

$$\mu\rho_{I,i} = (1 - \rho_{I,i})q_i, \quad (13)$$

and

$$w_{i,\ell} = T_i^\ell = \frac{\exp(\alpha n_{i,\ell})}{\sum_{\ell'} \exp(\alpha n_{i,\ell'})}, \quad (14)$$

where  $n_{i,\ell}$  can be written as  $n_{i,\ell} = \sum_{j=1}^N A_{ij}^\ell w_{j,\ell} \rho_{I,j}$  by the mean-field approximation. The stationary solutions of  $\rho_{I,i}$  and  $w_{i,\ell}$  can be obtained by numerically iterating Eq.(13) and Eq.(14) together with Eq.(8). Once  $\rho_{I,i}$  and  $w_{i,\ell}$  are obtained,  $\rho_I$  and  $\phi_\ell$  can be calculated by  $\rho_I = N^{-1} \sum_{i=1}^N \rho_{I,i}$  and  $\phi_\ell = N^{-1} \sum_{i=1}^N w_{i,\ell}$ , respectively. The comparison between the theory and simulations is shown in Fig.2. Obviously, the theory can reproduce qualitatively the main results of the simulations. Quantitatively, the simulations underestimate the range of the bistable region. One of the main reasons may be that near the boundaries of the bistable region the lifetime of one of the metastable states becomes short so that it cannot be fully sampled in the simulations.

For  $\beta$  lower than the epidemic threshold,  $\rho_{I,i} = 0$ , one notice that  $w_{i,\ell} = 1/\mathcal{L} \forall i, \ell$  is the only set solution of Eq.(14). Substituting  $w_{i,\ell} = 1/\mathcal{L}$  into Eq.(13) and then linearizing Eq.(13) around  $\rho_{I,i} = 0$ , we obtain the threshold value of the spreading rate,  $\beta_c$ , which is the inverse of the largest eigenvalue of the matrix  $\bar{\mathbf{A}}$ , defined as

$$\bar{\mathbf{A}} = \frac{1}{\mathcal{L}^2} \sum_{\ell=1}^{\mathcal{L}} \mathbf{A}^\ell, \quad (15)$$

such that

$$\beta_c = \frac{1}{\Lambda_{\max}(\bar{\mathbf{A}})}. \quad (16)$$

When the topologies of all the layers are the same,  $\mathbf{A}^1 = \dots = \mathbf{A}^\mathcal{L} = \mathbf{A}$ , the right boundary of the bistable region,  $\beta_{br}$ , can be derived analytically. Under such a case, it is not hard to check that  $w_{i,\ell} = 1/\mathcal{L}$  is always the set of solution of Eq.(14). The right boundary of the bistable region is determined by the condition under which the set of solution loses its stability. To this end, we need to write down the Jacobian matrix  $\mathbf{J}$  of Eq.(12). Since  $w_{i,\ell}$  satisfies the normalization condition  $\sum_{\ell} w_{i,\ell} = 1$ , only  $\mathcal{L} - 1$  variables among  $w_{i,\ell}$  ( $\ell = 1, \dots, \mathcal{L}$ ) are independent of each other. Therefore, we select  $w_{i,1}, \dots, w_{i,\mathcal{L}-1}$  as the independent variables, and thus  $\mathbf{J}$  is an  $(\mathcal{L} - 1)N$ -dimensional square. The entries of  $\mathbf{J}$  are given by the derivation of right hand side of Eq.(12) with respect to  $w_{i,\ell}$  at  $w_{i,\ell} = 1/\mathcal{L}$ . Denoting the right hand side of Eq.(12) by  $Dh_{i,\ell}$  with

$h_{i,\ell} = -w_{i,\ell} + T_i^\ell$ , the partial derivative of  $h_{i,\ell}$  with respect to  $w_{j,s}$  is given by

$$\begin{aligned} \frac{\partial h_{i,\ell}}{\partial w_{j,s}} = & -\delta_{ij}\delta_{\ell s} + \frac{\alpha A_{ij}\rho_{I,j}}{Z} \exp(\alpha n_{i,\ell}) \delta_{\ell s} \\ & - \frac{\alpha A_{ij}\rho_{I,j}}{Z^2} \exp(\alpha n_{i,\ell}) [\exp(\alpha n_{i,s}) - \exp(\alpha n_{i,\ell})] \end{aligned}$$

where  $Z = \sum_{\ell} \exp(\alpha n_{i,\ell})$  and  $\delta_{ij}$  is the Kronecker symbol defined as  $\delta_{ij} = 1$  if  $i = j$  and zero otherwise. At  $w_{i,\ell} = 1/\mathcal{L}$ ,  $n_{i,\ell} = \sum_j A_{ij}\rho_{I,j}^*/\mathcal{L}$  that is independent of the layer index  $\ell$ . This leads to

$$\left. \frac{\partial h_{i,\ell}}{\partial w_{j,s}} \right|_{w_{i,\ell}=1/\mathcal{L}} = -\delta_{ij}\delta_{\ell s} + \frac{1}{\mathcal{L}} \alpha A_{ij}\rho_{I,j}^* \delta_{\ell s} \quad (18)$$

Therefore, the Jacobian matrix  $\mathbf{J}$  can be written as the Kronecker product of two matrices,

$$\mathbf{J} = \mathbf{D}\mathbf{I} \otimes \mathbf{M}, \quad (19)$$

where  $\mathbf{I}$  is an  $(\mathcal{L} - 1)$ -dimensional identity matrix, and  $\mathbf{M}$  is an  $N$ -dimensional square whose entries are given by

$$M_{ij} = -\delta_{ij} + \frac{\alpha}{\mathcal{L}} A_{ij}\rho_{I,j}^*, \quad (20)$$

where  $\rho_{I,i}^*$  is determined by Eq.(13) at  $w_{i,\ell} = 1/\mathcal{L}$ , i.e.,

$$\rho_{I,i}^* = \frac{\beta}{\mathcal{L}} (1 - \rho_{I,i}^*) \sum_{j=1}^N A_{ij}\rho_{I,j}^*. \quad (21)$$

As mentioned above,  $\beta_{br}$  is the point at which the solution  $w_{i,\ell} = 1/\mathcal{L}$  loses its stability. This implies that  $\beta_{br}$  is determined whenever the largest eigenvalue of  $\mathbf{J}$  is equal to zero,  $\Lambda_{\max}(\mathbf{J}) = D\Lambda_{\max}(\mathbf{M}) = 0$ . Furthermore, as  $\rho_{I,i}^*$  is bounded between 0 and 1, we have  $\Lambda_{\max}(\mathbf{M}) \leq -1 + \frac{\alpha}{\mathcal{L}} \Lambda_{\max}(\mathbf{A})$  according to Wielandt's Theorem [56], and we arrive at a critical value of  $\alpha_c = \mathcal{L}/\Lambda_{\max}(\mathbf{A})$  in terms of the condition  $\Lambda_{\max}(\mathbf{M}) = 0$ . Therefore, a bistable phase can be observed only when  $\alpha > \alpha_c$ .

In general,  $\rho_{I,i}^*$  and  $\beta_{br}$  are obtained only by numerics. However, in the spirit of a simple mean-field theory we can derive their analytical results. Let  $\rho_I^* \equiv \rho_{I,i}^*$  and  $\langle k \rangle \equiv \sum_j A_{ij}$ , and thus  $\rho_I^* = 0$  or  $\rho_I^* = 1 - \mathcal{L}/(\beta \langle k \rangle)$  in terms of Eq.(21). Substituting the latter solution of  $\rho_I^*$  into Eq.(20) yields  $\Lambda_{\max}(\mathbf{M}) = -1 + \frac{\alpha}{\mathcal{L}} \left(1 - \frac{\mathcal{L}}{\beta \langle k \rangle}\right) \Lambda_{\max}(\mathbf{A}) = -1 + \frac{\alpha}{\mathcal{L}} \left(\langle k \rangle - \frac{\mathcal{L}}{\beta}\right)$ . Note that the simple mean-field theory is at work when the underlying network is degree-regular random network for which the largest eigenvalue of the adjacency matrix is  $\Lambda_{\max}(\mathbf{A}) = \langle k \rangle$ . Letting  $\Lambda_{\max}(\mathbf{M}) = 0$ , we obtain an analytical expression of  $\beta_{br}$ , given by

$$\beta_{br}^{SMF} = \frac{\mathcal{L}\alpha}{\alpha \langle k \rangle - \mathcal{L}}. \quad (22)$$

Since  $\beta_{br}^{SMF} \geq 0$  in Eq.(22), we obtain the value of  $\alpha_c$  in the simple mean-field theory,  $\alpha_c^{SMF} = \mathcal{L}/\langle k \rangle$ . We should note that the asymmetric solution of Eq.(14) for  $w_{i,\ell}$  can

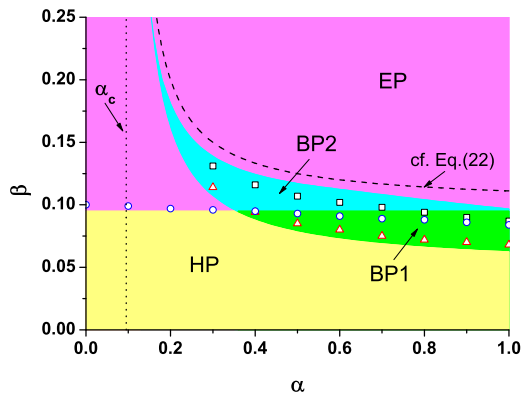


FIG. 3. Phase diagram for the SIS dynamics in a two-layer network. Each layer is consisted of an identical ER network with  $N = 50000$  and  $\langle k \rangle = 20$ . Four phases can be distinguished (encoded in color obtained from the mean-field theory): the healthy phase (HP), the endemic phase (EP), the bistable phase 1 (BP1) with the coexistence of the high-density EP and the HP, and the bistable phase 2 (BP2) with the coexistence of the high-density and low-density EPs. Vertical dotted line indicates to the critical value of  $\alpha$ ,  $\alpha_c$ , giving the lower bound for observing the bistable phase. Dashed line gives the right boundary of the bistable phase from the simple mean-field theory (cf. Eq.(22)). Symbols represents the simulation results for the boundaries of distinct phases ( $\circ$  for epidemic threshold,  $\triangle$  and  $\square$  for the left and right boundary of bistable region, respectively).

not be obtained analytically, such that the analytical determination for  $\beta_{bl}$  is in general impossible.

In Fig.3, we show the phase diagram in  $\beta \sim \alpha$  parametric spaces. The whole phase diagram can be divided into three regions: the HP, the BP, and the EP. The bistable region can be distinguished with two subregions. For the first bistable phase (BP1), the H-EP and the HP are coexisting. For the second bistable phase (BP2), the L-EP and the H-EP are coexisting.

Finally, we consider the case when the topologies of bilayer networks are not the same. In Fig.4(a) and Fig.4(b), we show  $\rho_I$  and  $\phi_1 - \phi_2$  as functions of  $\beta$  at  $\alpha = 0.3$ , where each layer is consisted of an ER networks with  $N = 5 \times 10^4$  nodes but with different average degrees,  $\langle k \rangle_1 = 18$  and  $\langle k \rangle_2 = 22$ . For  $\beta < 0.142$ , the case is similar to that in Fig.2 when the topologies of bilayer networks are the same. In the H-EP, the occupation probability in the second layer is dominant as we have set the average degree in this layer to be larger. Interestingly, a new bistable region appears for  $\beta > 0.142$ , as compared to Fig.2(b) and Fig.2(e). Within the new bistable region (called BP3), two different H-EPs coexist, corresponding to epidemic spreading widely either in the first layer or in the second layer. Due to the inequivalent topologies of bilayer networks, the prevalences are different. In Fig.4(c), we show the phase diagram.

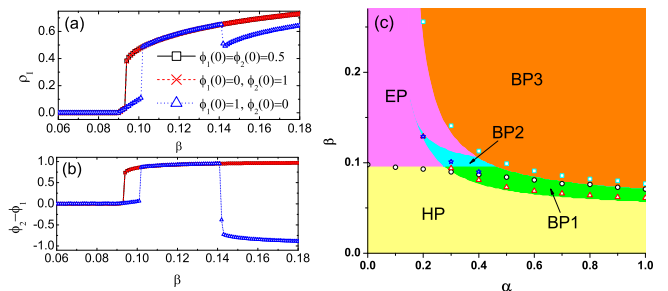


FIG. 4. The results for the SIS dynamics on a two-layer network with distinct topologies in each layer. Each layer is consisted of an ER network with the same number of nodes  $N = 5 \times 10^4$  but different average degrees:  $\langle k \rangle_1 = 18$  and  $\langle k \rangle_2 = 22$ . The density of infected individuals  $\rho_I$  (a) and the difference in occupying probabilities of individuals in each layer  $\phi_2 - \phi_1$  (b) as functions of  $\beta$  at  $\alpha = 0.3$ . (c) shows the phase diagram in  $\beta \sim \alpha$  parametric spaces. Due to topological difference in each layer an additional bistable region occurs in the upper-right corner (see Fig.3 for comparison). Symbols represent the simulation results of the boundaries of distinct phases ( $\circ$  for epidemic threshold, and  $\triangle$ ,  $\square$ , and  $\star$  for the boundaries of bistable region).

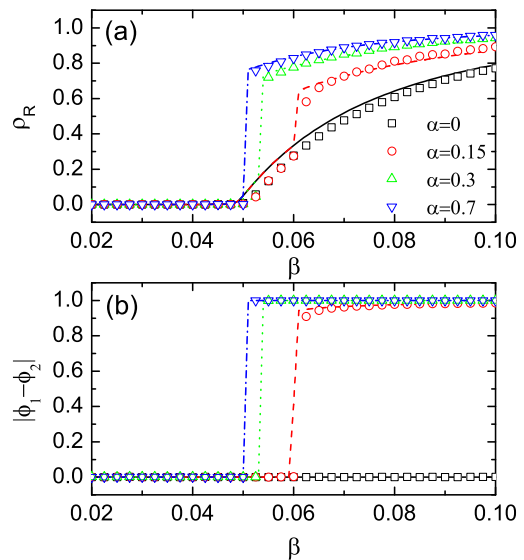


FIG. 5. The results for the SIR dynamics. The density of recovered individuals  $\rho_R$  (a) and the absolute value of difference in occupying probabilities  $|\phi_1 - \phi_2|$  (b) as functions of effective spreading rate  $\beta$  for four distinct values of  $\alpha$ : 0, 0.15, 0.3, and 0.7. Symbols and lines correspond to simulation and theoretical results, respectively. The multilayer network is consisted of two identical ER networks with  $N = 10^6$  and  $\langle k \rangle = 40$ .

#### IV. SIR DYNAMICS

In the SIR model, the number of infected individuals always tends to zero. The number of recovered individuals reaches only a limited number of individuals for low spreading rates and a finite fraction of the population

while for high spreading rates. In the thermodynamic limit, the prevalence  $\rho_R$  exhibits a transition from zero to nonzero as  $\beta$  increases. We run the SIR model in a very large multilayer network consisted of two identical ER random graphs with  $N = 10^6$  and  $\langle k \rangle = 40$ . The density of initial infection seeds are set to be much small,  $\rho_I(0) = 10^{-4}$ . We found that the way how to prepare the initial locations of individuals does not affect the ultimate prevalence, which may be related to irreversibility of the SIR model. In Fig.5(a) and Fig.5(b), we respectively show  $\rho_R$  and  $|\phi_1 - \phi_2|$  as functions of  $\beta$  for four distinct values of  $\alpha$ : 0, 0.15, 0.3, and 0.7. Similar to the SIS model, for low values of  $\alpha$  the model undergoes a usual continuous phase transition. For large enough values of  $\alpha$ , such as  $\alpha = 0.7$  shown in Fig.5, the model shows a discontinuous phase transition. While for the intermediate values of  $\alpha$ , such as  $\alpha = 0.15$  shown in Fig.5, the model first shows a continuous transition to a low-density prevalence and then abruptly jumps to a high-density prevalence. All the discontinuous transitions are also accompanied by the symmetry breaking in the occupation probabilities of individuals in each layer, as shown in Fig.5(b).

Theoretical analysis can be carried out in a similar way. Let us denote the probability that individual  $i$  is infected (recovered) at time  $t$  by  $\rho_{I,i}(t)$  ( $\rho_{R,i}(t)$ ). We can write down the time evolutions for  $\rho_{I,i}$  and  $\rho_{R,i}$ , given by

$$\frac{d\rho_{I,i}(t)}{dt} = (1 - \rho_{I,i}(t) - \rho_{R,i}(t)) q_i(t) - \mu\rho_{I,i}(t), \quad (23)$$

and

$$\frac{d\rho_{R,i}(t)}{dt} = \mu\rho_{I,i}(t), \quad (24)$$

where  $q_i(t)$  is also given by Eq.(8). The occupation probabilities of each individual in each layer,  $w_{i,\ell}(t)$ , are governed by Eq.(12) as well. Near phase transition,  $\rho_{R,i}$  is macroscopically infinitesimal, and thus Eq.(23) recovers to Eq.(11). Therefore, the threshold of the SIR model is also determined by Eq.(16). We numerically integrate Eqs.(23,24) and Eq.(12), and obtain the theoretical results, as indicated by lines in Fig.5. There are in excellent agreement between simulations and theory.

## V. CONCLUSIONS

In conclusion, we have proposed a spreading model in multilayer networks, and studied the nature of nonequilibrium phase transition as the effective spreading parameter varies. Our model is composed of a spreading process and a biased diffusion process between different layers. Using the SIS and SIR models as two paradigmatic examples of spreading dynamics, we found that the model in multilayer networks exhibits more abundant behaviors of phase transition than that in single-layer networks. For the SIS dynamics, when a biased parameter above a critical value the transition can be either continuous from the healthy phase to the low-prevalence endemic phase and then be discontinuous to the high-prevalence endemic phase, or be discontinuous directly from the healthy phase to the high-prevalence endemic phase, depending on the value of such a biased parameter and the distribution of initial positions of individuals. Between the two discontinuous transition points, the system is bistable and the occupation probabilities of individuals in each layer show a spontaneous symmetry breaking across these discontinuous transition points. For the SIR dynamics, we found that the nature of phase transition is also essentially changed as the biased parameter exceeds a critical value, similar to the case of SIS dynamics. However, we did not observe the bistability for the irreversible SIR model. Furthermore, we have developed an individual-based mean-field theory that can fully describe the nature of phase transitions in multilayer networks observed in simulations. Since the biased diffusion of individuals can lead to an abrupt explosion of epidemic, it will certainly provide a challenge as how to predict and control epidemic in real networks usually represented by multilayer networks [57].

## ACKNOWLEDGMENTS

We acknowledge the supports from the National Natural Science Foundation of China (Grants No. 61473001, No. 11875069) and the Natural Science Foundation of Anhui Province (Grant No. 1808085MF201).

- 
- [1] M. E. J. Newman, *SIAM Review* **45**, 167 (2003).
  - [2] S. Boccaletti, V. Latora, Y. Moreno, M. Chavez, and D.-U. Hwang, *Phys. Rep.* **424**, 175 (2006).
  - [3] A. Arenas, A. Díaz-Guilera, J. Kurths, Y. Moreno, and C. Zhou, *Phys. Rep.* **469**, 93 (2008).
  - [4] R. Pastor-Satorras, C. Castellano, P. Van Mieghem, and A. Vespignani, *Rev. Mod. Phys.* **87**, 925 (2015).
  - [5] M. Perc, J. J. Jordan, D. G. Rand, Z. Wang, S. Boccaletti, and A. Szolnoki, *Phys. Rep.* **687**, 1 (2017).
  - [6] S. N. Dorogovtsev, A. V. Goltsev, and J. F. F. Mendes, *Rev. Mod. Phys.* **80**, 1275 (2008).
  - [7] M. Leone, A. Vázquez, A. Vespignani, and R. Zecchina, *Eur. Phys. J. B* **28**, 191 (2002).
  - [8] S. N. Dorogovtsev, A. V. Goltsev, and J. F. F. Mendes, *Phys. Rev. E* **66**, 016104 (2002).
  - [9] S. Bradde, F. Caccioli, L. Dall'Asta, and G. Bianconi, *Phys. Rev. Lett.* **104**, 218701 (2010).
  - [10] R. Cohen, K. Erez, D. ben Avraham, and S. Havlin, *Phys. Rev. Lett.* **85**, 4626 (2000).
  - [11] D. S. Callaway, M. E. J. Newman, S. H. Strogatz, and D. J. Watts, *Phys. Rev. Lett.* **85**, 5468 (2000).
  - [12] R. Pastor-Satorras and A. Vespignani, *Phys. Rev. Lett.* **86**, 3200 (2001).

- [13] D. Achlioptas, R. M. D'Souza, and J. Spencer, *Science* **323**, 1453 (2009).
- [14] J. Gómez-Gardeñes, S. Gómez, A. Arenas, and Y. Moreno, *Phys. Rev. Lett.* **106**, 128701 (2011).
- [15] S. Boccaletti, J. A. Almendral, S. Guan, I. Leyva, Z. Liu, I. S. na Nadal, Z. Wang, and Y. Zou, *Phys. Rep.* **660**, 1 (2016).
- [16] M. Kivelä, A. Arenas, M. Barthelemy, J. P. Gleeson, Y. Moreno, and M. A. Porter, *J. Complex Netw.* **2**, 203 (2014).
- [17] G. Bianconi, *Multilayer networks: Structure and Function* (Oxford University Press, 2018).
- [18] S. Boccaletti, G. Bianconi, R. Criado, C. del Genio, J. Gómez-Gardeñes, M. Romance, I. Sendiña-Nadal, Z. Wang, and M. Zanin, *Phys. Rep.* **544**, 1 (2014).
- [19] S. V. Buldyrev, R. Parshani, G. Paul, H. E. Stanley, and S. Havlin, *Nature* **464**, 1025 (2010).
- [20] G. J. Baxter, S. N. Dorogovtsev, A. V. Goltsev, and J. F. F. Mendes, *Phys. Rev. Lett.* **109**, 248701 (2012).
- [21] S. Gómez, A. Díaz-Guilera, J. Gómez-Gardeñes, C. J. Pérez-Vicente, Y. Moreno, and A. Arenas, *Phys. Rev. Lett.* **110**, 028701 (2013).
- [22] F. Radicchi and A. Arenas, *Nat. Phys.* **9**, 717 (2013).
- [23] M. Salehi, R. Sharma, M. Marzolla, M. Magnani, P. Siyari, and D. Montesi, *IEEE Transactions on Network Science and Engineering* **2**, 65 (2015).
- [24] M. D. Domenico, C. Granell, M. A. Porter, and A. Arenas, *Nat. Phys.* **2**, 901 (2016).
- [25] G. F. de Arruda, F. A. Rodrigues, and Y. Moreno, *Phys. Rep.* **in press** (2018).
- [26] E. Cozzo, R. A. Baños, S. Meloni, and Y. Moreno, *Phys. Rev. E* **88**, 050801 (2013).
- [27] H. Wang, Q. Li, G. D'Agostino, S. Havlin, H. E. Stanley, and P. Van Mieghem, *Phys. Rev. E* **88**, 022801 (2013).
- [28] A. Saumell-Mendiola, M. A. Serrano, and M. Boguñá, *Phys. Rev. E* **86**, 026106 (2012).
- [29] G. Bianconi, *J. Stat. Mech.* p. 034001 (2017).
- [30] M. Dickison, S. Havlin, and H. E. Stanley, *Phys. Rev. E* **85**, 066109 (2012).
- [31] D. Soriano-Paños, L. Lotero, A. Arenas, and J. Gómez-Gardeñes, *Phys. Rev. X* **8**, 031039 (2018).
- [32] Q. Xuan, F. Du, L. Yu, and G. Chen, *Phys. Rev. E* **87**, 032809 (2013).
- [33] B. Wang, G. Tanaka, H. Suzuki, and K. Aihara, *Phys. Rev. E* **90**, 032806 (2014).
- [34] Z. Wang, L. Wang, A. Szolnoki, and M. Perc, *Eur. Phys. J. B* **88**, 124 (2015).
- [35] F. Battiston, M. Perc, and V. Latora, *New J. Phys.* **19**, 073017 (2017).
- [36] C. Xia, X. Li, Z. Wang, and M. Perc, *New J. Phys.* **20**, 075005 (2018).
- [37] J. Aguirre, R. Sevilla-Escoboza, R. Gutiérrez, D. Papo, and J. M. Buldú, *Phys. Rev. Lett.* **112**, 248701 (2014).
- [38] S. Majhi, M. Perc, and D. Ghosh, *Sci. Rep.* **6**, 39033 (2016).
- [39] C. I. del Genio, J. Gómez-Gardeñes, I. Bonamassa, and S. Boccaletti, *Sci. Adv.* **2**, e1601679 (2016).
- [40] M. Diakonova, M. San Miguel, and V. M. Eguíluz, *Phys. Rev. E* **89**, 062818 (2014).
- [41] M. Diakonova, V. Nicosia, V. Latora, and M. S. Miguel, *New J. Phys.* **18**, 023010 (2016).
- [42] A. Solé-Ribalta, S. Gómez, and A. Arenas, *Phys. Rev. Lett.* **116**, 108701 (2016).
- [43] S. Manfredi, E. Di Tucci, and V. Latora, *Phys. Rev. Lett.* **120**, 068301 (2018).
- [44] C. Granell, S. Gómez, and A. Arenas, *Phys. Rev. Lett.* **111**, 128701 (2013).
- [45] J.-Q. Kan and H.-F. Zhang, *Commun. Nonlinear Sci.* **44**, 193 (2017).
- [46] W. Wang, M. Tang, H. Yang, Y. Do, Y.-C. Lai, and G. Lee, *Sci. Rep.* **4**, 5097 (2014).
- [47] X. Zhang, S. Boccaletti, S. Guan, and Z. Liu, *Phys. Rev. Lett.* **114**, 038701 (2015).
- [48] V. Nicosia, P. S. Skardal, A. Arenas, and V. Latora, *Phys. Rev. Lett.* **118**, 138302 (2017).
- [49] F. Velásquez-Rojas and F. Vazquez, *Phys. Rev. E* **95**, 052315 (2017).
- [50] M. A. Pires, A. L. Oestereich, and N. Crokidakis, *J. Stat. Mech.* p. 053407 (2018).
- [51] J. Jiang and T. Zhou, *Sci. Rep.* **8**, 1629 (2018).
- [52] Z. Su, W. Wang, L. Li, H. Stanley, and L. A. Braunstein, *New J. Phys.* **20**, 053053 (2018).
- [53] X. Chen, R. Wang, M. Tang, S. Cai, H. Stanley, and L. A. Braunstein, *New J. Phys.* **20**, 013007 (2018).
- [54] I. Mishkovski, M. Mirchev, S. Scepanovic, and L. Kocarev, *IEEE Transactions on Circuits and Systems I: Regular Papers* **64**, 2761 (2017).
- [55] P. Erdős and A. Rényi, *Publ. Math. Inst. Hung. Acad. Sci* **5**, 17 (1960).
- [56] I. S. Gradshteyn and I. M. Ryzhik, *Tables of Integrals, Series, and Products, 5th ed* (CA: Academic Press, 1979).
- [57] Z. Wang, C. T. Bauch, S. Bhattacharyya, A. d'Onofrio, P. Manfredi, M. Perc, N. Perra, M. Salathé, and D. Zhao, *Phys. Rep.* **664**, 1 (2016).